

Medium-induced cascade in expanding media

Souvik Priyam Adhya^a Carlos A. Salgado^b Martin Spousta^a Konrad Tywoniuk^c

^a*Institute of Particle and Nuclear Physics, Faculty of Mathematics and Physics, Charles University, V Holesovickach 2, 180 00 Prague 8, Czech Republic*

^b*Instituto Galego de Física de Altas Enerxías IGFAE, Universidade de Santiago de Compostela, E-15782 Galicia-Spain*

^c*Department of Physics and Technology, University of Bergen, 5007 Bergen, Norway*

E-mail: souvik@ipnp.mff.cuni.cz, carlos.salgado@usc.es,
martin.spousta@mff.cuni.cz, konrad.tywoniuk@uib.no

ABSTRACT: A detailed insight into the interplay between parton energy loss and the way how deconfined medium created in heavy-ion collisions expands is of a great importance for improving the understanding of the jet quenching phenomenon. In this paper we study the impact of the expansion of deconfined medium on single-gluon emission spectra and the jet suppression factor (Q_{AA}) within the BDMPs-Z formalism. We calculate these quantities for three types of media, namely static medium, exponentially decaying medium and Bjorken expanding medium. The distribution of medium-induced gluons and the jet Q_{AA} are calculated using the evaluation of in-medium evolution with splitting kernels derived from the gluon emission spectra. A universal behavior of splitting kernels is derived for low- x and high- x regimes in the asymptote of large times and its impact on the resulting jet Q_{AA} is discussed. For the full phase-space of the radiation where the results are obtained by a numerical solution of the evolution equation, it is shown that the impact of the medium expansion can be scaled out from the jet Q_{AA} by an effective quenching parameter. This effective quenching parameter is however different from the time-averaged quenching parameter that can be derived for each type of expanding media. We find sizable differences among the values of the effective quenching parameter that point to the importance of the medium expansion for precise modeling of the jet quenching phenomenon.

KEYWORDS: Perturbative QCD, LPM effect, Jet quenching, Expanding QGP

Contents

| | | |
|----------|--|-----------|
| 1 | Introduction | 1 |
| 2 | Emission spectrum and rate in an expanding medium | 2 |
| 2.1 | Static medium | 4 |
| 2.2 | Exponentially decaying medium | 5 |
| 2.3 | Bjorken expanding medium | 7 |
| 2.4 | Properties of the emission spectrum and rate | 9 |
| 3 | Rate equation for expanding medium | 11 |
| 4 | Moments of $D(x, \tau)$ and the jet suppression factor | 12 |
| 5 | Conclusions & outlook | 16 |

1 Introduction

Measurements of jets in heavy-ion collisions at RHIC and the LHC revealed many interesting results. The production of inclusive jets was found to be strongly suppressed in central heavy-ion collisions with respect to proton-proton collisions [1–4] as a direct consequence of the parton energy loss. It was shown that the fragmentation patterns of jets are significantly modified in heavy-ion collisions and that the lost energy is transferred to soft particles, predominantly emitted away from the jet axis [5–10]. These are only few of important results (for review see e.g. Ref. [11]) which however clearly demonstrate that the rich phenomenon of jet quenching calls for an accurate theoretical description.

In this paper we study one particular aspect of the jet quenching, namely the impact of the medium expansion on the rate of stimulated radiation and the related in-medium medium-induced branching. The starting point of the calculations presented here is the formalism for propagation and radiation in a dense medium within the BDMPS-Z framework [12–15]. This allows to resum multiple interactions with the medium through a Schrödinger equation for the relevant in-medium correlator, see [16, 17]. The solution can be obtained via direct numerical evaluation [18–20] or as an expansion in terms of the medium opacity [21–23]. Currently, we work within the approximation of multiple-soft scattering, also referred to as the “dipole” or “harmonic oscillator” approximation [24, 25], when the resummation for dense media can be performed analytically and that describes well the regime of typical gluon emissions [26].¹

Multiple scattering in expanding media was analyzed in [29] and later in [24, 30, 31] (see also [32] for a numerical solution in this case). These calculations indicate an important

¹Improvements to account for rare emissions can also be systematically included [27, 28].

impact of the finite expanding medium on the observable quantities such as the nuclear modification factor of hadrons. Interesting features, such as the scaling of gluon energy spectra in expanding media with average transport coefficient, were early identified [24, 30]. This scaling indicates that some of the main features of the medium-induced spectra remain unchanged no matter the underlying density profile of the background medium.

These approaches have been successfully confronted with experimental data on jet and single-inclusive hadron suppression [32–34] with the aim to reliably extract properties of the dense medium created in heavy-ion collisions. Phenomenological studies aim ultimately at establishing the relation between the jet quenching parameter and the energy density of the quark gluon plasma [35] which, according to perturbative estimates, should scale like $\hat{q}/T^3 \sim 2(\epsilon/T^4)^{3/4}$ [36].² Since the energy density is expected to change dramatically during the life-time of the system, jet modifications carry an imprint of this evolution. This prompts us to improve the theoretical description of jet quenching in expanding media.

In this work, rather than attempting a full phenomenological description of experimental data, we focus on shedding light on the universal features of radiative energy loss, and deviations from them. We extend previous studies to obtain single-inclusive gluon spectra and related in-medium emission rates, and use these to obtain the jet suppression factor for three different types of expanding medium. However, we do not attempt to model the fluctuations related to the production point of the jet or its substructure. The in-medium distributions are found using numerical solution of the evolution equation for gluon emission spectra introduced in [38, 39] with the important input from a unified treatment of expanding media derived in [40]. This allows us to study specific properties and scaling of single-inclusive gluon emission spectra and jet suppression factor which can be compared to recent measurements done at the LHC. While many analyses of in-medium evolution so far have focused on static media [38, 41], it is also important to establish whether the qualitative features observed there, such as the rapid transfer of energy to low-energy modes [42, 43], can be carried over to expanding cases.

The paper is organized as follows. Section 2 introduces emission spectra and rate of emissions in an expanding medium for three different types of media and discusses their properties. Section 3 provides calculations of medium evolved gluon emission spectra obtained using the evolution equation with input rates from Section 2. In Section 4, the moments of gluon spectra are calculated allowing to obtain the jet suppression factor, Q_{AA} , for different types of expanding media. The scaling properties of the jet Q_{AA} with respect to the transport properties of the expanding media are discussed. Section 5 provides a summary and outlook.

2 Emission spectrum and rate in an expanding medium

Calculations of medium-induced gluon radiation in the evolving media presented in this paper are done in the limit of multiple soft scatterings and follow the BDMPS-Z formalism [12–15]. The starting point is the gluon emission spectrum radiated from an initial massless

²See also [37] for other ideas.

parton with energy p (we only consider gluon splitting at the moment). The final expression can be cast in a general form as [40]

$$\frac{dI}{dz} = \frac{\alpha_s}{\pi} P(z) \ln |c(0)|, \quad (2.1)$$

where $P(z) \equiv P_{gg}(z) = 2N_c[1 - z(1 - z)]^2/z(1 - z)$ is the Altarelli-Parisi splitting function. The strong coupling constant α_s runs with the typical transverse momentum accumulated during the emission, $k_\perp \sim (z(1 - z)p\hat{q})^{1/4}$, but in the remainder of the paper we will treat it as a constant, $\alpha_s = 0.3$.

In Eq. (2.1), $c(t)$ is a function that encodes information about the medium and its expansion [40]. It is the solution of a differential equation

$$\frac{d^2 c(t)}{dt^2} + \Omega^2(t)c(t) = 0, \quad (2.2)$$

where $\Omega(t)$ is a time-dependent, complex frequency. For our purposes (gluon splitting), this frequency is simply given by

$$\Omega^2(t) = -i \frac{\hat{q}_{\text{eff}}(t)}{2z(1 - z)p}, \quad (2.3)$$

where the effective jet quenching parameter is given by $\hat{q}_{\text{eff}}(t) = [1 - z(1 - z)]\hat{q}(t)$. The boundary conditions are such that $c(t)$ approaches 1 at $t \rightarrow \infty$; this realizes the fact that the particle ends up in a vacuum state, i.e. $\hat{q} \rightarrow 0$ and therefore $\Omega(t) \rightarrow 0$ as $t \rightarrow \infty$. On the other hand, $t = 0$ corresponds to the position of the hard scattering that produces the hard particle sourcing the splitting.

We can also derive an emission rate, defined as

$$\mathcal{K}(z, \tau) \equiv \frac{dI}{dz d\tau}, \quad (2.4)$$

per unit “time” τ . This is a dimensionless number defined as

$$\tau = \sqrt{\frac{\hat{q}_0}{p}} L, \quad (2.5)$$

where L is the distance the initial parton travels through the medium. The parameter $\hat{q}_0 = \hat{q}(t_0)$ is the initial value of the jet quenching parameter. The rate $\mathcal{K}(z, \tau)$ is an input to calculations of medium evolved gluon spectra, which will be discussed in Section 3.

For expanding media, the quenching parameter is time dependent, $\hat{q} = \hat{q}(t)$. The average quenching parameter for a given type of the expanding medium is

$$\langle \hat{q} \rangle = \frac{2}{L^2} \int_{t_0}^{L+t_0} dt (t - t_0) \hat{q}(t), \quad (2.6)$$

where t_0 corresponds to the time-scale for the onset of quenching effects, i.e. $\hat{q}(t < t_0) = 0$. In this work we will consider three examples of medium evolution, differing by $\hat{q}(t)$ profiles and therefore with different $c(0)$. These are the static medium, exponentially decaying

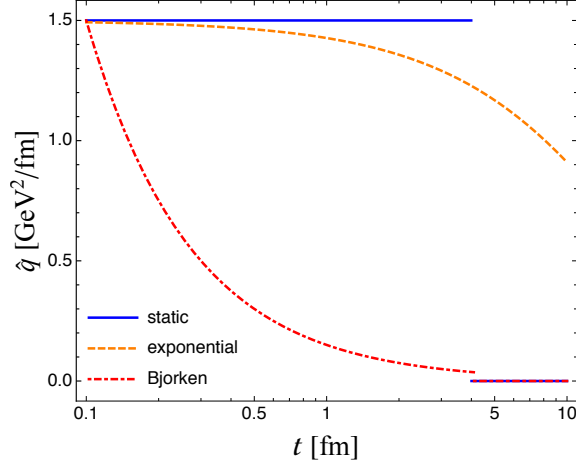


Figure 1. The time dependence of the \hat{q} coefficient for the different expanding scenarios considered in this paper: a static medium (blue, solid), exponentially decaying medium (orange, dashed) and the Bjorken expanding medium (red, dot-dashed).

medium and the Bjorken expanding medium. The time dependence of \hat{q} for these different media is fully specified later in this section and summarized in Fig. 1. For the former two examples we can safely put $t_0 = 0$ while for the Bjorken scenario, where the energy density and therefore also $\hat{q}(t)$ diverges at small times, we have to use a finite $t_0 = 0.1$ fm. Moreover, the exponentially decreasing spectrum is extending up to $t = \infty$, which automatically regularizes $\hat{q}(t)$ at late times, and it is therefore natural to define the average jet quenching parameter as

$$\langle \hat{q} \rangle_{\text{exp}} = \frac{2}{L^2} \int_0^\infty dt t \hat{q}(t), \quad (2.7)$$

in this case. The reference values for the jet quenching parameter at initial time and the size of the medium used in this section are $\hat{q}_0 = 1.5 \text{ GeV}^2/\text{fm}$ and $L = 4 \text{ fm}$, respectively. Emission spectra and rates for these examples as well as their properties are detailed in the remainder of this section.

2.1 Static medium

For a static medium, $\hat{q}(t) = \hat{q}_0$ for $t < L$ and vanishes at later times, and obviously $\langle \hat{q} \rangle = \hat{q}_0$ as well. In this case, $\Omega^2(t) = \Omega_0^2$, see below, at $t < L$ and $\Omega^2(t) = 0$ at $t > L$. The spectrum is given by [12–15]

$$\frac{dI}{dz} = \frac{\alpha_s}{\pi} P(z) \text{Re} \ln \cos \Omega_0 L, \quad (2.8)$$

where

$$\Omega_0 L = \sqrt{\frac{-i \hat{q}_0}{2} \frac{\kappa(z)}{p}} L = \frac{1-i}{2} \kappa(z) \tau, \quad (2.9)$$

and $\kappa(z) = \sqrt{[1 - z(1 - z)]/[z(1 - z)]}$. Focusing on the small- z limit, $z \ll 1$, and defining the gluon frequency $\omega = zp$, we see that the spectrum has two regimes, namely

$$\omega \frac{dI}{d\omega} \simeq 2\bar{\alpha} \begin{cases} \sqrt{\frac{\omega_c}{2\omega}} & \text{for } \omega \ll \omega_c, \\ \frac{1}{12} \left(\frac{\omega_c}{\omega}\right)^2 & \text{for } \omega \gg \omega_c, \end{cases} \quad (2.10)$$

where $\bar{\alpha} \equiv \alpha_s N_c / \pi$ and the characteristic (hard) gluon frequency is

$$\omega_c = \frac{1}{2} \hat{q}_0 L^2. \quad (2.11)$$

The $\omega^{-1/2}$ behavior at low energies is a consequence of the LPM interference effect, and applies for gluons with formation times shorter than the medium length, $t_f \sim \sqrt{\omega/\hat{q}} < L$. This essential feature fundamentally impacts the resulting distribution of medium-induced parton cascade [38]. Furthermore, in this regime the spectrum is proportional to the in-medium path length, $\omega dI/d\omega \propto L$. At long formation times, $t_f \sim \sqrt{\omega/\hat{q}} > L$, or $\omega > \omega_c$, the spectrum is strongly suppressed.

Returning now to finite z , in terms of the evolution variable τ , the rate then becomes

$$\mathcal{K}(z, \tau) = \frac{\alpha_s}{2\pi} P(z) \kappa(z) \operatorname{Re} \left[(i - 1) \tan \left(\frac{1 - i}{2} \kappa(z) \tau \right) \right]. \quad (2.12)$$

It is useful also to recall the “soft” limit of this spectrum that will be used for comparison later on. We are interested in the regime $\kappa(z)\tau \sim \tau/\sqrt{z} \gg 1$, for large τ or for $z \ll \tau^2$, where we can expand cosine in Eq. (2.8) to obtain

$$\left. \frac{dI}{dz} \right|_{\tau \gg \sqrt{z}} \simeq \frac{\alpha_s}{2\pi} P(z) \kappa(z) \tau, \quad (2.13)$$

where the rate $\mathcal{K}(z, \tau) \simeq \frac{\alpha_s}{2\pi} P(z) \kappa(z)$ is constant in “time”. In order to highlight the features of the rate, and corresponding distribution of gluons emitted in the medium, we will further simplify this expression by neglecting all z -dependence apart from the (apparent) singular behavior in $z \rightarrow 0$ and $z \rightarrow 1$. In this case, the rate reads

$$\mathcal{K}(z, \tau)|_{\text{sing}} = \frac{\bar{\alpha}}{[z(1 - z)]^{3/2}}. \quad (2.14)$$

This can also be found by considering the limit of large times τ , conversely small z , directly in Eq. (2.12), where $\lim_{x \rightarrow \infty} \tan(1 - i)x = -i$ and hence the rate tends to constant, time-independent value at large times. It turns out that the medium evolution of the gluon distribution is exactly solvable using Eq. (2.13) [38], which makes it an interesting limiting case.

2.2 Exponentially decaying medium

For exponentially decaying media the profile of the jet quenching parameter is given by

$$\hat{q}(t) = \hat{q}_0 e^{-t/L}. \quad (2.15)$$

Note that in this case the average parameter, according to Eq. (2.7), is $\langle \hat{q} \rangle_{\text{exp}}/\hat{q}_0 \approx 2$, i.e. twice as big as for the static medium. This is a consequence of the fact that, although exponentially suppressed, the quenching is allowed to take place over very long distances.

The solution of $c(t)$ satisfying the boundary conditions at $t \rightarrow \infty$ is readily found, and in this case the spectrum is given by

$$\frac{dI}{dz} = \frac{\alpha_s}{\pi} P(z) \text{Re} \ln J_0(2\Omega_0 L), \quad (2.16)$$

where $J_0(z)$ is a Bessel function of the first kind and $\Omega_0 L$ is given in Eq. (2.9). We point out the factor 2 appearing inside the Bessel function, that highlights some of the peculiar features of this particular scenario. The rate then becomes

$$\mathcal{K}(z, \tau) = \frac{\alpha_s}{\pi} P(z) \kappa(z) \text{Re} \left[(i-1) \frac{J_1((1-i)\kappa(z)\tau)}{J_0((1-i)\kappa(z)\tau)} \right]. \quad (2.17)$$

We notice again the ratio of Bessel functions tend to a constant value at large times $\lim_{x \rightarrow \infty} J_1((1-i)x)/J_0((1-i)x) = -i$. However, given the profile defined in Eq. (2.15), this limiting value is twice as large as for the static case,

$$\lim_{\tau \rightarrow \infty} \mathcal{K}_{\text{exp}}(z, \tau) = 2 \lim_{\tau \rightarrow \infty} \mathcal{K}_{\text{static}}(z, \tau). \quad (2.18)$$

This mismatch can in principle be remedied by rescaling medium parameters in Eq. (2.15), e.g. $L \rightarrow L/2$.

To put these insights onto firmer theoretical ground and reveal the scaling features of the spectrum and rate, let us presently analyze the leading behavior arising in the limit of $z \rightarrow 0$ and $z \rightarrow 1$. We will therefore approximate $\kappa(z) \approx 1/\sqrt{z(1-z)}$ and $P(z) \approx 2N_c/(z(1-z))$, and employ the asymptotic form of the Bessel functions for large arguments. With these approximations the emission spectrum (2.16) can be written as,

$$\begin{aligned} \left. \frac{dI}{dz} \right|_{\text{sing}} &\simeq \frac{2\bar{\alpha}}{z(1-z)} \left\{ \text{Re} \ln \cos \left[(1-i) \sqrt{\frac{\hat{q}_0 L^2}{z(1-z)p}} - \frac{\pi}{4} \right] + \frac{1}{4} \ln \left(\frac{2z(1-z)p}{\pi^2 \hat{q}_0 L^2} \right) \right\} \\ &\approx \frac{2\bar{\alpha}}{z(1-z)} \text{Re} \ln \cos \left[\frac{1-i}{2} \sqrt{\frac{2\langle \hat{q} \rangle L^2}{z(1-z)p}} - \frac{\pi}{4} \right], \end{aligned} \quad (2.19)$$

where in the second step we neglected the second term in the small or large z limit and introduced the average $\langle \hat{q} \rangle_{\text{exp}} = 2\hat{q}_0$. The subscript “sing” is meant to indicate that we neglect all finite z corrections away from the singularities at $z \rightarrow 0$ and $z \rightarrow 1$. We observe that, apart from the factor $\pi/4$ under the cosine, there is only a factor 2 difference under the square root between the exponentially decaying medium and a static one, cf. Eq. (2.8). While this difference could be absorbed into a modified average \hat{q} , it will nevertheless spoil the ideal scaling with $\langle \hat{q} \rangle$ of the spectrum in the soft regime.

Similarly, the rate (2.17) can be approximated as,

$$\begin{aligned} \mathcal{K}(z, \tau)|_{\text{sing}} &\simeq \frac{2\bar{\alpha}}{[z(1-z)]^{3/2}} \text{Re} (i-1) \tan \left[(1-i) \frac{\tau}{\sqrt{z(1-z)}} - \frac{\pi}{4} \right], \\ &\approx \frac{2\bar{\alpha}}{[z(1-z)]^{3/2}}, \end{aligned} \quad (2.20)$$

where in the second step we additionally assumed that $z \ll \tau^2$. On comparing with Eq. (2.14), we note an overall factor 2 difference of the rate. Somewhat surprisingly, in this idealized situation all the effects of the expansion can therefore be absorbed into a rate with a modified coupling constant.

2.3 Bjorken expanding medium

This type of the medium is motivated by the Bjorken expansion, which leads to the drop of energy density $\varepsilon(t)$ with proper time as $\varepsilon(t) = \varepsilon(t_0)(t_0/t)^{4/3}$ for massless relativistic particles. Since $\hat{q} \propto \varepsilon^{3/4}$, one can therefore model the time dependence of the jet quenching parameter as [29],

$$\hat{q}(t) = \begin{cases} 0 & \text{for } t < t_0, \\ \hat{q}_0(t_0/t)^\alpha & \text{for } t_0 < t < L + t_0, \\ 0 & \text{for } L + t_0 < t. \end{cases} \quad (2.21)$$

The $\alpha \neq 1$ generalizes the above mentioned Bjorken expansion. The average value of $\langle \hat{q} \rangle$ is in this case dependent on the ratio t_0/L . For the typical values $t_0 = 0.1$ fm, $L = 4$ fm, and $\alpha = 1$ we find $\langle \hat{q} \rangle_{\text{Bjork}}/\hat{q}_0 \approx 0.05$, i.e. the expansion reduces the average quenching parameter by a factor of 20.

The spectra for generic power-law expansions characterized by α were analyzed in [24, 29, 40]. The spectrum is given by

$$\frac{dI}{dz} = \frac{\alpha_s}{\pi} P(z) \text{Re} \ln \left[\left(\frac{t_0}{L + t_0} \right)^{1/2} \frac{J_\nu(z_0)Y_{\nu-1}(z_L) - Y_\nu(z_0)J_{\nu-1}(z_L)}{J_\nu(z_L)Y_{\nu-1}(z_L) - Y_\nu(z_L)J_{\nu-1}(z_L)} \right], \quad (2.22)$$

for $\alpha < 2$ with $\nu \equiv 1/(2 - \alpha)$, and where

$$z_0 \equiv 2\nu \frac{1-i}{2} \kappa(z) \sqrt{\frac{\hat{q}_0}{p}} t_0 = \nu(1-i)\kappa(z)\tau_0, \quad (2.23)$$

$$z_L \equiv 2\nu \frac{1-i}{2} \kappa(z) \sqrt{\frac{\hat{q}_0}{p}} \sqrt{t_0(L + t_0)} = \nu(1-i)\kappa(z)\sqrt{\tau_0(\tau + \tau_0)}, \quad (2.24)$$

where $\tau_0 = \sqrt{\hat{q}_0/p}t_0$. In what follows $\alpha = 1$ (and $\nu = 1$) implying

$$\frac{dI}{dz} = \frac{\alpha_s}{\pi} P(z) \text{Re} \ln \left[\left(\frac{t_0}{L + t_0} \right)^{1/2} \frac{J_1(z_0)Y_0(z_L) - Y_1(z_0)J_0(z_L)}{J_1(z_L)Y_0(z_L) - Y_1(z_L)J_0(z_L)} \right], \quad (2.25)$$

and the rate becomes

$$\mathcal{K}(z, \tau) = \frac{\alpha_s}{2\pi} P(z) \kappa(z) \sqrt{\frac{\tau_0}{\tau + \tau_0}} \text{Re} \left[(1-i) \frac{J_1(z_L)Y_1(z_0) - J_1(z_0)Y_1(z_L)}{J_1(z_0)Y_0(z_L) - J_0(z_L)Y_1(z_0)} \right]. \quad (2.26)$$

We point out that this rate depends explicitly on τ_0 as well as on τ . The long-time behavior of this scenario stands out compared to the other two cases analyzed above. While the

factor inside the square brackets in Eq. (2.26) goes to a constant, i.e. $\lim_{\tau \rightarrow \infty} \text{Re}[\dots] = 1$, the square root in front leads to a power-like decay of the rate at large times, i.e.

$$\lim_{\tau \rightarrow \infty} \mathcal{K}(z, \tau) = \frac{\alpha_s}{2\pi} P(z) \kappa(z) \sqrt{\frac{\tau_0}{\tau}}. \quad (2.27)$$

However, this can be also obtained for sufficiently small z , i.e. $z \ll z_c \equiv \tau_0 \tau$. In fact, for these small z values the properties of the Bjorken expanding and the static case, where $z_c \equiv \tau^2$ are quite similar, i.e. $\mathcal{K}_{\text{static}}(z_c, \tau) \approx \mathcal{K}_{\text{Bjork}}(z_c, \tau) \propto \tau^{-1}$.

Once again, we now turn to the “singular” behavior, see the previous sub-section, of the spectrum and rate in order to extract the scaling features. We employ the asymptotic forms of the Bessel functions to calculate the emission spectra for the Bjorken medium Eq. (2.22) in the limit of small or large z . We finally get

$$\begin{aligned} \left. \frac{dI}{dz} \right|_{\text{sing}} &\simeq \frac{2\bar{\alpha}}{z(1-z)} \text{Re} \ln \left[\sqrt{\frac{t_0}{L+t_0}} \cos \left((1-i) \sqrt{\frac{\hat{q}_0 t_0 L}{z(1-z)p}} \right) \right], \\ &\simeq \frac{2\bar{\alpha}}{z(1-z)} \left[\text{Re} \ln \cos \left(\frac{1-i}{2} \sqrt{\frac{2\langle \hat{q} \rangle L^2}{z(1-z)p}} \right) + \frac{1}{2} \ln \frac{t_0}{L} \right] \end{aligned} \quad (2.28)$$

where in the second step we introduced the average quenching parameter $\langle \hat{q} \rangle_{\text{Bjork}} = 2\hat{q}_0 t_0 / L$. In this case, the spectrum contains an additive term when compared to its equivalent static expression (2.8) that can be neglected at small- z . In addition, we see a similar factor of 2 mismatch of the average \hat{q} as for the exponential case.

Similarly, the rate (2.26) can be approximated as,

$$\begin{aligned} \mathcal{K}(z, \tau)|_{\text{sing}} &\simeq \frac{\bar{\alpha}}{[z(1-z)]^{3/2}} \sqrt{\frac{\tau_0}{\tau_0 + \tau}} \text{Re}(i-1) \tan \left[(1-i) \sqrt{\frac{\tau_0 \tau}{z(1-z)}} \right], \\ &\approx \frac{\bar{\alpha}}{[z(1-z)]^{3/2}} \sqrt{\frac{\tau_0}{\tau}}, \end{aligned} \quad (2.29)$$

where in the second line we additionally assumed $z \ll \tau_0 \tau$. Comparing the above equation with (2.12), we note several differences. Overall, similarly to the exponential case, there is a factor of 2 difference in the argument of the tangent. Additionally, the rate depends on τ in a different way than in the static case. This is manifested in the extra pre-factor $\sim \sqrt{\tau_0/\tau}$ and the factor $\sqrt{\tau_0 \tau}$ in the argument of the tangent. This additional factor will indeed break the naive scaling of the Bjorken rate with the static and exponential media.

However, the additional time-dependent pre-factor can be absorbed into a redefinition of the evolution time in the rate equations. Introducing

$$\tau^* = \sqrt{\tau_0 \tau}, \quad (2.30)$$

with $2d\tau^* = \sqrt{\tau_0/\tau} d\tau$, we can recast the rate as

$$\mathcal{K}(z, \tau^*)|_{\text{sing}} \approx \frac{2\bar{\alpha}}{[z(1-z)]^{3/2}}. \quad (2.31)$$

In summary, we have showed that the Bjorken expanding medium leads to a qualitatively different time-dependence of the rate which is expected to further affect the resulting distribution of medium-induced gluons.

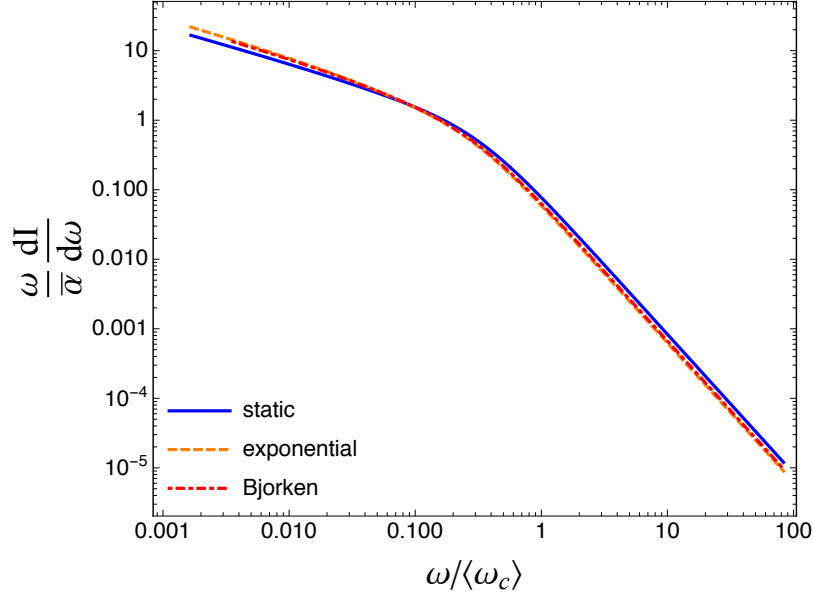


Figure 2. Spectrum of medium induced gluons $\omega dI/d\omega$ (in the limit $z \ll 1$) scaled by $\bar{\alpha} = \alpha_s N_c / \pi$ and plotted as a function of the gluon energy rescaled by $\langle\omega_c\rangle = \langle\hat{q}\rangle L^2/2$. The plotting options are the same as in Fig. 1.

2.4 Properties of the emission spectrum and rate

We compare the spectra of medium-induced gluon in Fig. 2. We have plotted the spectrum $\omega dI/d\omega$ versus $\omega/\langle\omega_c\rangle$, i.e. the energy rescaled by the maximal available gluon energy in the medium $\langle\omega_c\rangle \equiv \langle\hat{q}\rangle L^2/2$. We see that the Bjorken model (red, dot-dashed curve in Fig. 2) respects the scaling, as first discussed in [24, 30]. The exponential profile, with $\langle\hat{q}\rangle$ defined as in Eq. (2.7), also obeys the scaling, cf. the (orange) dashed curve in Fig. 2. This confirms that the properties of the spectra for different expanding profiles are well understood in terms of a proper re-scaling of the medium parameters. These scaling properties have also been derived analytically for both the spectrum and the corresponding rate in Secs. 2.2 and 2.3.

In Fig. 3, we compare the resulting rates $\mathcal{K}(z, \tau)$ for two values of z , $z = 0.001$ and $z = 0.4$ (however, note that $\mathcal{K}(1-z, \tau) = \mathcal{K}(z, \tau)$). The splitting rate for the static medium in the soft limit is constant, see (grey) dotted curves. For the exponential and full static cases, the splitting rate starts to grow from zero at $\tau = 0$, then it saturates at $\tau \sim \sqrt{z}$. For the exponentially decaying medium, the rate saturates at slightly larger times compared to the static case, which is a consequence of limiting behavior of the ratio of Bessel's function in Eq. (2.17). In contrast, the rate for Bjorken expanding medium converges to zero at large times. While the ratio of Bessel's function in Eq. (2.26) converges to unity for $\tau \sim z/\tau_0$, the presence of the factor $\sqrt{\tau_0/(\tau_0 + \tau)}$ leads to the dumping of the splitting rate for $\tau > \tau_0$. See also Secs. 2.2 and 2.3 for further details on the analytical properties of the scaling. The values of $\mathcal{K}(z, \tau)$ at large τ are larger for the exponential case than for the Bjorken case due to a consistent treatment of length of the medium (see definition Eq. (2.15)). As

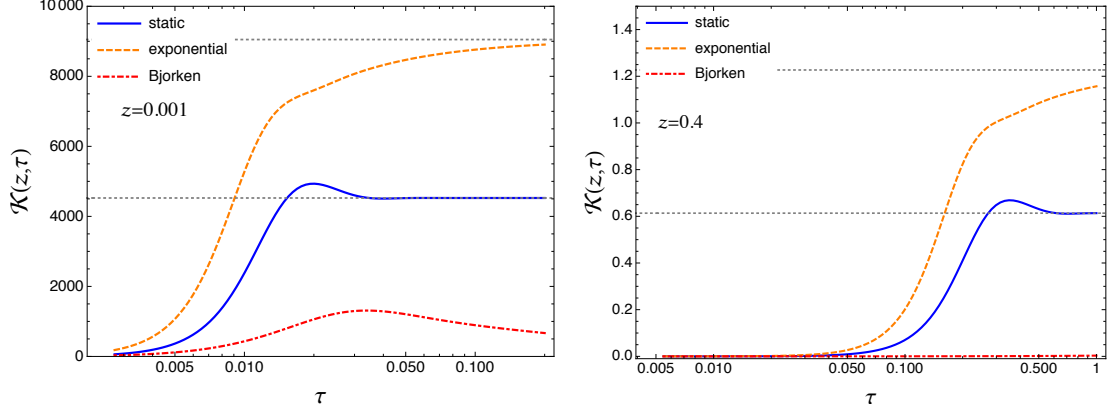


Figure 3. Gluon emission rate for two values of z , $z = 0.001$ (left) and $z = 0.4$ (right), as a function of the “time” τ . For the Bjorken case, we have chosen $\tau_0 = \sqrt{\hat{q}_0/p}t_0 \approx 0.005$. The plotting options are the same as in Fig. 1. We have also plotted the rate from the static, soft approximation, resulting from Eq. (2.13), and additionally scaled by a factor 2 to reproduce the long-time limit of Eq. (2.17).

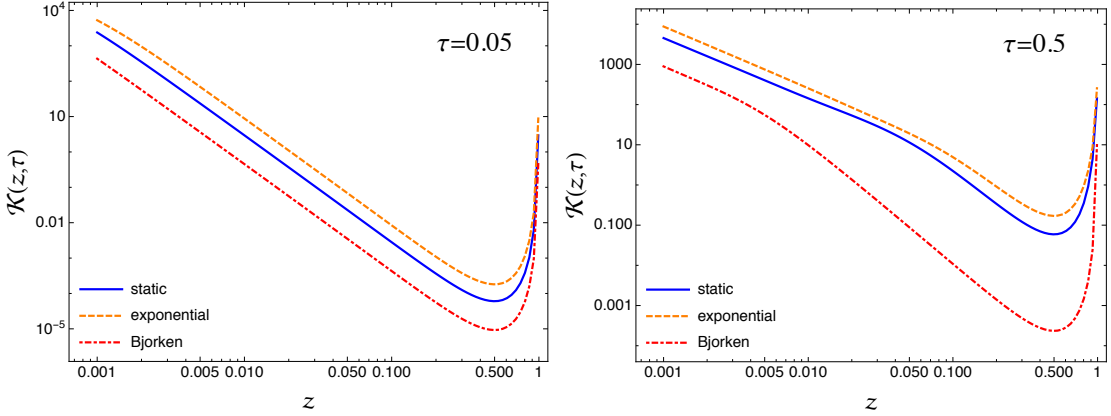


Figure 4. Gluon emission rate for two values of τ , $\tau = 0.05$ (left) and $\tau = 0.5$ (right), as a function of the momentum fraction z . The plotting options are the same as in Fig. 1.

discussed above, this mismatch can in principle be corrected by the proper redefinition of the profile defined in Eq. (2.15).

Finally, Fig. 4 shows a comparison of $\mathcal{K}(z, \tau)$ for two values of τ , $\tau = 0.05$ and $\tau = 0.5$, plotted as a function of the momentum fraction z . While at high values of z the rates for different profiles differ significantly, at the low- z values they all have the same, universal slope which is a consequence of the $P(z)\kappa(z)$ factor present in splitting rates of all the profiles which diverges for $z \rightarrow 0$ as $z^{-3/2}$. We therefore expect to recover a universal behavior of the resulting parton branching evolution for expanding media in the soft gluon regime.

3 Rate equation for expanding medium

Equipped with the rate of emissions, we can now turn to the task of resumming multiple gluon emissions in the medium. In a large medium, possible interference terms are suppressed [44, 45], and the resummation is enforced via a kinetic rate equation. The evolution equation for the energy distribution of medium-induced gluons, $D(x, \tau) = x \, dN/dx$, is given by [38, 39]

$$\frac{\partial D(x, \tau)}{\partial \tau} = \int_0^1 dz \, \mathcal{K}(z, \tau) \left[\sqrt{\frac{z}{x}} D\left(\frac{x}{z}, \tau\right) \Theta(z - x) - \frac{z}{\sqrt{x}} D(x, \tau) \right]. \quad (3.1)$$

The initial value of the $D(x, \tau)$ is a δ -function at $x = 1$ which characterizes the initial single color charge entering the evolving medium. Furthermore, conservation of energy implies

$$\int_0^1 dx \, D(x, \tau) = 1. \quad (3.2)$$

While this is formally violated due to the soft singularity at $x = 0$, this can be reinstated by assuming the accumulation of energy at the thermal scale $x \sim T/p$ where elastic rescattering leads to thermalization [42].

The rate equation Eq. (3.1) was solved numerically for the static medium, exponentially decaying medium, and the Bjorken case introduced in Sec. 2. In this section and onwards, the medium parameters are $\hat{q}_0 = 1 \text{ GeV}^2/\text{fm}$ and $L = 4 \text{ fm}$ if not indicated otherwise. The resulting distributions of $D(x)$ are shown for three representative values of τ in Fig. 5, see figure caption for further details. Despite the differences observed in the rates, at low x , all the $D(x)$ distributions converge to a universal scaling with $1/\sqrt{x}$ which is a consequence of the low- x behavior discussed in Sec. 2.4 driven by a presence of factors $P(z)\kappa(z)$ in all the splitting rates. The magnitude of the effects is different and is expected to scale with the average parameter $\langle \hat{q} \rangle$ which is hierarchically $\langle \hat{q} \rangle_{\text{exp}} > \langle \hat{q} \rangle_{\text{static}} > \langle \hat{q} \rangle_{\text{Bjork}}$ (for the choice of parameters used here). At high- x , which predominantly drives the jet suppression factor, see Sec. 4, the reduction of $D(x, \tau)$ is the strongest for the exponentially decaying medium and the weakest for the Bjorken case, according to the established hierarchy of $\langle \hat{q} \rangle$ for the parameters used here.

As a check of our numerical routine, we have also evaluated the distribution for the static soft limit, i.e. where we use Eq. (2.14) as the splitting rate. These results can be compared with the known analytical solution [38],

$$D_{\text{sing}}(x, \tau) = \frac{\bar{\alpha}\tau}{\sqrt{x}(1-x)^{3/2}} e^{-\pi \frac{\bar{\alpha}^2 \tau^2}{1-x}}, \quad (3.3)$$

where the sub-script refers to the “singular” rate in Eq. (2.14), see also [46]. The numerical and analytical results are plotted in Fig. 5 as the solid (black) and dashed (black) curves and we see a good agreement over a wide range in x . In this situation, the energy stored in the spectrum decreases exponentially with τ , $\mathcal{E}(\tau) = \int_0^1 dx \, D(x, \tau) = e^{-\pi \bar{\alpha}^2 \tau^2}$ [38].³ Small deviation between the numerical and analytical results impacting the physics observables discussed in the next section are covered by systematic uncertainties obtained from varying the discrete parameterization in the numerical calculation.

³Note that the authors [38] use directly $\tilde{\tau} = \bar{\alpha}\tau$ as the evolution time.

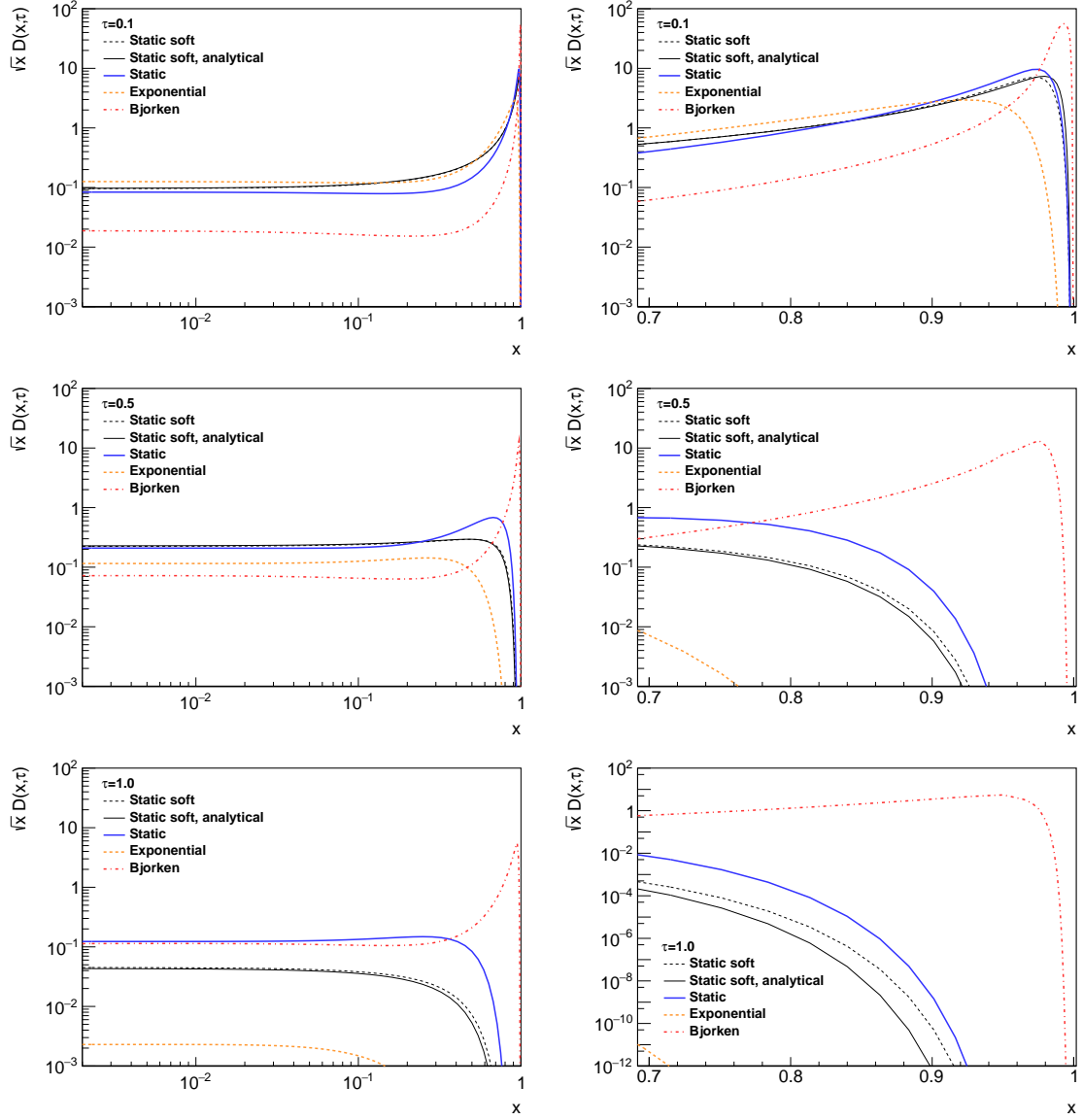


Figure 5. Medium induced gluon distribution $D(x)$ for three different values of τ and four types of medium expansion calculated numerically, static soft (dashed black), static (solid blue), exponential (dashed orange), and Bjorken (dashed-dotted red), and for the soft limit of the static medium calculated analytically (solid black). Left panels show the full distribution, right panels zoom in the high- x region.

4 Moments of $D(x, \tau)$ and the jet suppression factor

One of key observables quantifying the inclusive jet suppression is the jet nuclear modification factor, measured by LHC experiments [1–4]. The yield for the inclusive jet suppression can be obtained as a convolution of the $D(x, \tau)$ distribution with the initial parton spectra,

$$\frac{d\sigma_{AA}}{dp_T} = \int_0^\infty dp'_T \int_0^1 dx \delta(p_T - xp'_T) D\left(x, \tau \equiv \sqrt{\hat{q}_0/p'_T} L\right) \frac{d\sigma_0}{dp'_T}, \quad (4.1)$$

see e.g. [24, 33, 47]. Note that the evolution time τ now depends on the unknown initial energy of the parton. The initial parton spectra can be approximated by a power law, $d\sigma_0/dp_T \propto p_T^{-n}$. In this case, the jet suppression factor $Q_{AA}(p_T) = (d\sigma_{AA}/dp_T)/(d\sigma_0/dp_T)$, is

$$Q_{AA}(p_T) = \int_0^1 dx x^{n-1} D(x, \sqrt{x}\tau), \quad (4.2)$$

where now $\tau = \sqrt{\hat{q}_0/p_T}L$, as before. For the Bjorken model, the distribution has additionally a dependence on the initial time τ_0 , $D(x, \tau_0, \tau)$, that is also rescaled by the (unknown) initial p_T . However, in our current implementation, we have not implemented this exact dependence and choose to show an uncertainty band related to the starting time τ_0 .⁴

Let us focus for a moment on the analytical solution of the rate equation given by Eq. (3.3). At the present stage, it is illuminating to change variables as $1 - \epsilon/p_T = x$, where ϵ has the meaning of the energy lost by the particle due to medium-induced emissions. In this case,

$$Q_{AA}(p_T) = \int_0^{p_T} d\epsilon \left(1 - \frac{\epsilon}{p_T}\right)^{n-1} \sqrt{\frac{\omega_s}{\epsilon^3}} e^{-\frac{\pi\omega}{\epsilon} \left(1 - \frac{\epsilon}{p_T}\right)}, \quad (4.3)$$

where $\omega_s = \bar{\alpha}^2 \hat{q}_0 L^2$ is the scale of soft, multiple gluon emissions. In the limit of $\omega_c \ll p_T$, this expression can be approximated by

$$Q_{AA}(p_T) \approx \int_0^\infty d\epsilon e^{-\nu\epsilon} \sqrt{\frac{\omega_s}{\epsilon^3}} e^{-\frac{\pi\omega}{\epsilon}} = e^{-2\sqrt{\pi\omega_s\nu}}, \quad (4.4)$$

where $\nu = (n-1)/p_T$. This is nothing else than the (inverse) Laplace transform of the energy loss distribution $\mathcal{P}(\epsilon) = \sqrt{\omega_s/\epsilon^3} e^{-\pi\omega_s/\epsilon}$. This quantity is normalized $\int_0^\infty d\epsilon \mathcal{P}(\epsilon) = 1$. We have checked numerically that the approximation in going from Eq. (4.3) to (4.4) is valid to a few percent over a large range of p_T .

Jet suppression from scaling. Let us then apply the results found in Secs. 2.2 and 2.3 regarding the scaling features of the rates for the different medium profiles to gain further analytical insight into the results for the medium-induced gluon distribution and suppression factor Q_{AA} . We have extracted these features by only retaining the “singular” parts of the spectrum. Hence, the full solution that includes finite- z and finite length effects should be expected to deviate. However, we expect the qualitative features to be visible in the numerical results that will be discussed in detail below.

For the exponential case, Eq. (2.20) indicates that the solution to the rate equation is given by Eq. (3.3) with $\bar{\alpha} \rightarrow 2\bar{\alpha}$ or $\hat{q}_0 \rightarrow 4\hat{q}_0$, namely

$$D(x, \tau) \approx \frac{2\bar{\alpha}\tau}{\sqrt{x}} e^{-4\pi\bar{\alpha}^2\tau^2}, \quad (4.5)$$

⁴ Error bands shown on the plots later in this section were obtained by varying the parameters of numerical procedures such as the number of points on a discrete grid or the resolution parameter, and, for the Bjorken case, by varying τ_0 by a factor of 4 up and down starting from $\tau_0 = 0.03$ at $p_T \simeq 50$ GeV.

where we focus on the small- x regime where finite-length corrections should be smaller. This also implies that, for the same $\bar{\alpha}$ \hat{q}_0 , the ratio of suppression factors is,

$$\frac{Q_{AA}^{\text{exp}}}{Q_{AA}^{\text{static}}} \simeq \exp \left[-2\bar{\alpha} \sqrt{\pi \hat{q}_0 L^2 (n-1)/p_T} \right]. \quad (4.6)$$

We therefore expect that all effects of the expansion can be absorbed into the proper rescaling of the parameters.

For the Bjorken scenario, the situation is slightly more complicated. However, our result for the “singular” rate (2.31) indicates that we can write the final solution for the medium-induced gluon distribution as

$$D(x, \tau) \approx \frac{2\bar{\alpha} \sqrt{\tau_0 \tau}}{\sqrt{x}} e^{-4\pi \bar{\alpha}^2 \tau_0 \tau}, \quad (4.7)$$

in the small- x regime. We note that the evolution time is now $\tau^* = \sqrt{\tau_0 \tau}$ rather than τ itself. Interestingly, this gives a difference in suppression factors to the static case as

$$\frac{Q_{AA}^{\text{Bjork}}}{Q_{AA}^{\text{static}}} \simeq \exp \left[-2\bar{\alpha} \sqrt{\pi \hat{q}_0 L^2 (n-1)/p_T} \left(2\sqrt{\frac{t_0}{L}} - 1 \right) \right]. \quad (4.8)$$

We conclude that in the case of the Bjorken expansion there is not universal way of rescaling the parameters to arrive at the results of the static medium. Instead, approximate scaling can be achieved for given values of the medium parameters, including t_0 .

Numerical results on jet suppression. For our phenomenological applications, we include only one parton species (gluons) in the hard spectrum with $n = 5.6$ [48]. The distribution $D(x, \tau)$ is found by a numerical solution to Eq. (3.1), as described in Sec. 3. Due to above described limitations, the Q_{AA} calculated here is just a proxy for the nuclear modification factor, R_{AA} , measured by experiments. To make this explicit we use symbol Q_{AA} instead of R_{AA} in this paper.

We start our discussion by fixing a common reference value of the jet quenching parameter at initial time $\hat{q}_0 = 1 \text{ GeV}^2/\text{fm} = 0.2 \text{ GeV}^3$ for all three profiles. We show the resulting Q_{AA} distributions in Fig. 6, plotted for two values of $\omega_c = 60 \text{ GeV}$ (left) and $\omega_c = 100 \text{ GeV}$ (right), where $\omega_c = \hat{q}_0 L^2/2$. From this we extract the path-length in the medium to be $L = 5 \text{ fm}$ and 6.3 fm , respectively. Apart from the common value of \hat{q}_0 at initial time, a large difference can be seen for different media due to the varying rate of expansion in Fig. 6. In order to guide the eye, we have also plotted experimental data for high- p_T (anti- k_t , $R = 0.4$) jet suppression [2]. As an illustration, we will use the $\omega_c = 100 \text{ GeV}$ and $\hat{q}_0 = 0.2 \text{ GeV}^3$ values extracted from the static medium, see Fig. 6 (right), as reference values for the remaining studies.

The impact of the difference in the type of the medium expansion on the Q_{AA} can to a certain degree be scaled out by replacing the \hat{q}_0 such that the average $\langle \hat{q} \rangle$, given by Eq. (2.6), is the same for all the profiles. While for the static medium we trivially have that the average jet quenching parameter equals the initial one, $\langle \hat{q} \rangle = \hat{q}_0$, this does not hold for the case of expanding media where $\langle \hat{q} \rangle_{\text{exp}} \approx 2\hat{q}_0$ for an exponential medium profile and

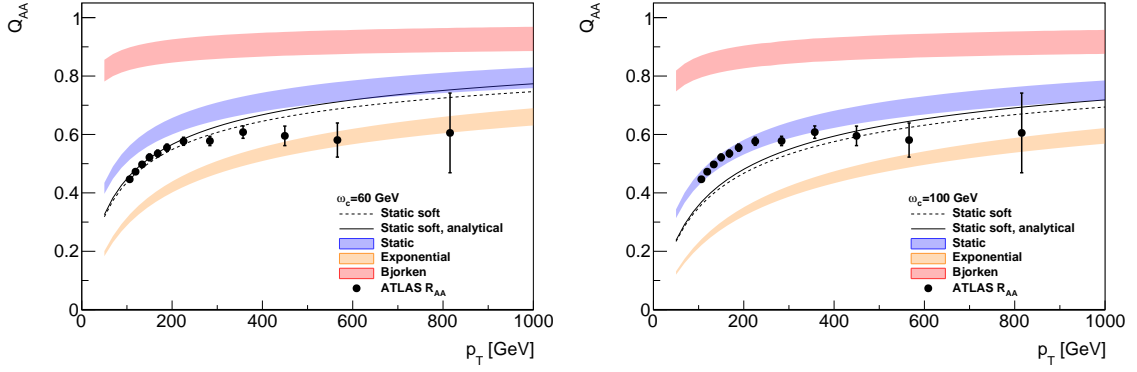


Figure 6. The jet suppression factor for four types of medium expansion calculated numerically, static soft (dashed line), static (blue), exponential (orange), and Bjorken (red), and the soft limit of the static medium calculated analytically (full line). We plot Q_{AA} for $\omega_c = 60$ GeV (left) and $\omega_c = 100$ GeV (right). ATLAS data taken from [2].

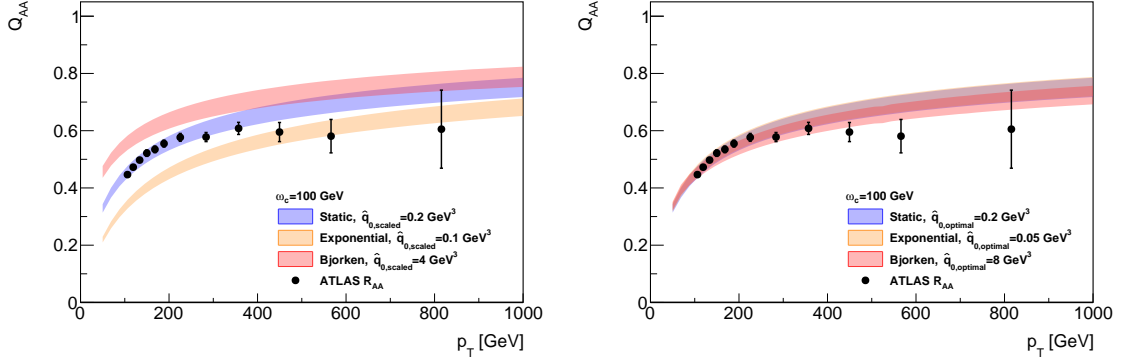


Figure 7. The jet suppression factor for four types of medium expansion calculated numerically, static soft (dashed line), static (blue), exponential (orange), and Bjorken (red), and the soft limit of the static medium calculated analytically (full line). On the left: Q_{AA} calculated for $\langle \hat{q} \rangle_{\text{static}} = \langle \hat{q} \rangle_{\text{exp}} = \langle \hat{q} \rangle_{\text{Bjork}}$. On the right: Q_{AA} for values $\hat{q}_0 = \hat{q}_{0,\text{optimal}}$ fitted to experimental data from ATLAS [2], keeping ω_c constant. See legend or Tab. 1 for reference values.

$\langle \hat{q} \rangle_{\text{Bjork}} \approx 0.05 \hat{q}_0$ for the Bjorken-like profile. The new \hat{q}_0 for which $\langle \hat{q} \rangle$ is the same for all the profiles is labeled here $\hat{q}_{0,\text{scaled}}$. The left panel of Fig. 7 shows the resulting suppression for the same $\langle \hat{q} \rangle$ for the three cases (corresponding to $\hat{q}_{0,\text{scaled}} = 0.2$ (static), 0.1 (exponential), and 4 (Bjorken) GeV^3 , respectively, resulting in $\langle \hat{q} \rangle_{\text{static}} = \langle \hat{q} \rangle_{\text{exp}} = \langle \hat{q} \rangle_{\text{Bjork}}$). Since the dependence of dI/dz on τ is different for different types of the medium expansion, kernels of the evolution as well as resulting $D(x, \tau)$ distribution may differ even if the dI/dz have the same dependence on z . This is indeed seen in the left panel of Fig. 7 where the Q_{AA} factors for different types of the medium expansion differ by roughly a factor $\sim 1.3 - 2$ (at high- and low- p_T) between the largest and the smallest quenching factors.

On the other hand, it is possible to find an effective quenching parameter, $\hat{q}_{0,\text{optimal}}$ *independently* in the three scenarios that minimizes the difference among the jet Q_{AA} fac-

| Quenching parameter [GeV ³] | static | exponential | Bjorken |
|---|--------|-------------|---------|
| \hat{q}_0 | 0.2 | 0.2 | 0.2 |
| $\hat{q}_{0,\text{scaled}}$ | 0.2 | 0.1 | 4 |
| $\hat{q}_{0,\text{optimal}}$ | 0.2 | 0.05 | 8 |

Table 1. Table showing a comparison of the values of the jet quenching coefficients at initial time t_0 , \hat{q}_0 , for the different medium profiles. The first row corresponds to the reference values used in Fig. 6. The second row corresponds to the re-scaled values of \hat{q}_0 given the same average value of $\langle \hat{q} \rangle$ for the three cases, see Fig. 7 (left). Finally, the values in the third row corresponds to the optimal initial densities found through a χ^2 minimization to fit the data on jet suppression, see Fig. 7 (right).

tors. The values of $\hat{q}_{0,\text{optimal}}$ were obtained by a χ^2 minimization of the difference between the jet suppression data and theory calculations by keeping $\omega_c = \hat{q}_0 L^2/2 = 100$ GeV fixed. The resulting distributions of jet Q_{AA} are shown in the right panel of Fig. 7 with $\hat{q}_{0,\text{optimal}}$ being approximately 0.2, 0.05, and 8 GeV³ for static soft, exponential and Bjorken type of the expansion, respectively. Note that the values of $\hat{q}_{0,\text{scaled}}$ and $\hat{q}_{0,\text{optimal}}$ are quite different for expanding media, see Tab. 1. We suspect that this difference could also be affected by the steepness of the hard spectrum. This exercise shows that, having fixed the relevant medium parameters, the p_T -behavior is quite similar for the different medium expansion scenarios (small differences can perhaps be seen at high- p_T).

5 Conclusions & outlook

Three types of the medium expansion were studied within the framework of multiple soft scattering, namely the static medium, exponentially decaying medium and Bjorken-like expanding medium. The spectra and rates of induced gluon emissions were evaluated and the distribution of medium-induced gluons were calculated using the evaluation of in-medium evolution (Eq. (3.1)) with splitting kernels obtained from rates of induced gluon emissions. Single-inclusive gluon distributions were then used to calculate the jet suppression factor Q_{AA} , see Eq. (4.2).

A universal behavior of splitting kernels is derived for low- x and high- x regimes in the asymptote of large times (see Eq. (2.14), Eq. (2.20), and Eq. (2.29)). It is shown that the impact of the medium expansion on the resulting jet Q_{AA} in this limit can be absorbed into the proper rescaling of the parameters for the case of the exponential expansion (see Eq. (4.6)), while the same is not possible for the case of the Bjorken expansion (see Eq. (4.8)).

For the full evolution in time and full phase-space of the radiation, the results are obtained by a numerical solution of the evolution equation. The evolved distributions are shown to obey a $1/\sqrt{x}$ scaling for all the studied types of expansion signaling a universal behavior with reduced sensitivity to the details of the medium expansion. It was found that the impact of the medium expansion cannot be scaled out by using the average quenching parameter, see Fig. 7 (left) when taking into account the full evolution. Hence, although

many features of the medium-induced spectrum, see Fig. 2, and the single-inclusive distributions at low- x , see Fig. 5, are common to all studied medium expansion scenarios, the details of the high- x behavior of $D(x, \tau)$, that ultimately drives the quenching factor Q_{AA} , is still relatively sensitive to the details of medium expansion. Values of quenching parameter at initial time $\hat{q}_{0,\text{optimal}}$ that minimize the differences in the jet Q_{AA} among the different types of the expansion were also found. Large difference between the theoretically motivated scaled \hat{q}_0 values and $\hat{q}_{0,\text{optimal}}$, see also Tab. 1, indicate the importance of taking into account the medium expansion in precise modeling of the jet quenching phenomenon.

The extracted values of the initial \hat{q}_0 obtained in this paper cannot be taken at face value, given the fitting procedure described above. Several improvements, such as including proper quark and gluon jet fractions [48], using a comprehensive emission rate [28, 32], accounting for quark and gluon coupled induced branching [41] and including the effect of in-medium jet fragmentation (Sudakov suppression) [49], are planned to be included for future phenomenological applications of other observables, such as v_2 at high- p_T .

Acknowledgments

KT is supported by a Starting Grant from Trond Mohn Foundation (BFS2018REK01) and the University of Bergen. CAS is supported by Ministerio de Ciencia e Innovación of Spain under project FPA2017-83814-P; Unidad de Excelencia María de Maetzu under project MDM-2016-0692; ERC-2018-ADG-835105 YoctoLHC; and Xunta de Galicia (Consellería de Educación) and FEDER. SPA and MS are supported by Grant Agency of the Czech Republic under grant 18-12859Y, by the Ministry of Education, Youth and Sports of the Czech Republic under grant LTT 17018, and by Charles University grant UNCE/SCI/013.

References

- [1] ATLAS collaboration, *Measurements of the Nuclear Modification Factor for Jets in Pb+Pb Collisions at $\sqrt{s_{NN}} = 2.76$ TeV with the ATLAS Detector*, *Phys. Rev. Lett.* **114** (2015) 072302 [[1411.2357](#)].
- [2] ATLAS collaboration, *Measurement of the nuclear modification factor for inclusive jets in Pb+Pb collisions at $\sqrt{s_{NN}} = 5.02$ TeV with the ATLAS detector*, *Phys. Lett.* **B790** (2019) 108 [[1805.05635](#)].
- [3] CMS collaboration, *Measurement of inclusive jet cross sections in pp and PbPb collisions at $\sqrt{s_{NN}} = 2.76$ TeV*, *Phys. Rev.* **C96** (2017) 015202 [[1609.05383](#)].
- [4] ALICE collaboration, *Measurements of inclusive jet spectra in pp and central Pb-Pb collisions at $\sqrt{s_{NN}} = 5.02$ TeV*, [1909.09718](#).
- [5] CMS COLLABORATION collaboration, *Observation and studies of jet quenching in PbPb collisions at nucleon-nucleon center-of-mass energy = 2.76 TeV*, *Phys.Rev.* **C84** (2011) 024906 [[1102.1957](#)].
- [6] CMS collaboration, *Measurement of Jet Fragmentation in PbPb and pp Collisions at $\sqrt{s_{NN}} = 2.76$ TeV*, *Phys. Rev.* **C90** (2014) 024908 [[1406.0932](#)].

- [7] ATLAS collaboration, *Measurement of inclusive jet charged-particle fragmentation functions in Pb+Pb collisions at $\sqrt{s_{NN}}=2.76$ TeV with the ATLAS detector*, *Phys. Lett.* **B739** (2014) 320 [[1406.2979](#)].
- [8] ATLAS collaboration, *Measurement of jet fragmentation in Pb+Pb and pp collisions at $\sqrt{s_{NN}} = 2.76$ TeV with the ATLAS detector at the LHC*, *Eur. Phys. J.* **C77** (2017) 379 [[1702.00674](#)].
- [9] ATLAS collaboration, *Measurement of jet fragmentation in Pb+Pb and pp collisions at $\sqrt{s_{NN}} = 5.02$ TeV with the ATLAS detector*, *Phys. Rev.* **C98** (2018) 024908 [[1805.05424](#)].
- [10] CMS collaboration, *Jet Shapes of Isolated Photon-Tagged Jets in Pb-Pb and pp Collisions at $\sqrt{s_{NN}} = 5.02$ TeV*, *Phys. Rev. Lett.* **122** (2019) 152001 [[1809.08602](#)].
- [11] M. Connors, C. Nattrass, R. Reed and S. Salur, *Jet measurements in heavy ion physics*, *Rev. Mod. Phys.* **90** (2018) 025005 [[1705.01974](#)].
- [12] R. Baier, Y. L. Dokshitzer, A. H. Mueller, S. Peigne and D. Schiff, *Radiative energy loss of high-energy quarks and gluons in a finite volume quark - gluon plasma*, *Nucl.Phys.* **B483** (1997) 291 [[hep-ph/9607355](#)].
- [13] R. Baier, Y. L. Dokshitzer, A. H. Mueller, S. Peigne and D. Schiff, *Radiative energy loss and $p(T)$ broadening of high-energy partons in nuclei*, *Nucl.Phys.* **B484** (1997) 265.
- [14] B. Zakharov, *Fully quantum treatment of the Landau-Pomeranchuk-Migdal effect in QED and QCD*, *JETP Lett.* **63** (1996) 952.
- [15] B. Zakharov, *Radiative energy loss of high-energy quarks in finite size nuclear matter and quark - gluon plasma*, *JETP Lett.* **65** (1997) 615 [[hep-ph/9704255](#)].
- [16] Y. Mehtar-Tani, J. G. Milhano and K. Tywoniuk, *Jet physics in heavy-ion collisions*, *Int. J. Mod. Phys.* **A28** (2013) 1340013 [[1302.2579](#)].
- [17] J.-P. Blaizot and Y. Mehtar-Tani, *Jet Structure in Heavy Ion Collisions*, *Int. J. Mod. Phys.* **E24** (2015) 1530012 [[1503.05958](#)].
- [18] S. Caron-Huot and C. Gale, *Finite-size effects on the radiative energy loss of a fast parton in hot and dense strongly interacting matter*, *Phys.Rev.* **C82** (2010) 064902 [[1006.2379](#)].
- [19] X. Feal and R. Vazquez, *Intensity of gluon bremsstrahlung in a finite plasma*, *Phys. Rev.* **D98** (2018) 074029 [[1811.01591](#)].
- [20] W. Ke, Y. Xu and S. A. Bass, *A modified-Boltzmann approach for modeling the hot QCD medium-induced splitting vertices in the deep LPM region*, [1810.08177](#).
- [21] U. A. Wiedemann, *Gluon radiation off hard quarks in a nuclear environment: Opacity expansion*, *Nucl. Phys.* **B588** (2000) 303 [[hep-ph/0005129](#)].
- [22] M. Gyulassy, P. Levai and I. Vitev, *NonAbelian energy loss at finite opacity*, *Phys.Rev.Lett.* **85** (2000) 5535 [[nucl-th/0005032](#)].
- [23] M. D. Sievert, I. Vitev and B. Yoon, *A complete set of in-medium splitting functions to any order in opacity*, [1903.06170](#).
- [24] C. A. Salgado and U. A. Wiedemann, *Calculating quenching weights*, *Phys.Rev.* **D68** (2003) 014008 [[hep-ph/0302184](#)].
- [25] N. Armesto, C. A. Salgado and U. A. Wiedemann, *Medium induced gluon radiation off massive quarks fills the dead cone*, *Phys. Rev.* **D69** (2004) 114003 [[hep-ph/0312106](#)].

- [26] P. B. Arnold, *High-energy gluon bremsstrahlung in a finite medium: harmonic oscillator versus single scattering approximation*, *Phys. Rev.* **D80** (2009) 025004 [[0903.1081](#)].
- [27] Y. Mehtar-Tani, *Gluon bremsstrahlung in finite media beyond multiple soft scattering approximation*, *JHEP* **07** (2019) 057 [[1903.00506](#)].
- [28] Y. Mehtar-Tani and K. Tywoniuk, *Improved opacity expansion for medium-induced parton splitting*, [1910.02032](#).
- [29] R. Baier, Y. L. Dokshitzer, A. H. Mueller and D. Schiff, *Radiative energy loss of high-energy partons traversing an expanding QCD plasma*, *Phys. Rev.* **C58** (1998) 1706 [[hep-ph/9803473](#)].
- [30] C. A. Salgado and U. A. Wiedemann, *A Dynamical scaling law for jet tomography*, *Phys.Rev.Lett.* **89** (2002) 092303 [[hep-ph/0204221](#)].
- [31] B. G. Zakharov, *Parton energy loss in an expanding quark-gluon plasma: Radiative versus collisional*, *JETP Lett.* **86** (2007) 444 [[0708.0816](#)].
- [32] X. Feal, C. A. Salgado and R. A. Vazquez, *Jet quenching tests of the QCD Equation of State*, [1911.01309](#).
- [33] Y. Mehtar-Tani and K. Tywoniuk, *Jet (de)coherence in PbPb collisions at the LHC*, *Phys. Lett.* **B744** (2015) 284 [[1401.8293](#)].
- [34] F. Arleo, *Quenching of Hadron Spectra in Heavy Ion Collisions at the LHC*, *Phys. Rev. Lett.* **119** (2017) 062302 [[1703.10852](#)].
- [35] S. Borsanyi, G. Endrodi, Z. Fodor, A. Jakovac, S. D. Katz, S. Krieg et al., *The QCD equation of state with dynamical quarks*, *JHEP* **11** (2010) 077 [[1007.2580](#)].
- [36] R. Baier, *Jet quenching*, *Nucl. Phys.* **A715** (2003) 209 [[hep-ph/0209038](#)].
- [37] A. Majumder, B. Muller and X.-N. Wang, *Small shear viscosity of a quark-gluon plasma implies strong jet quenching*, *Phys. Rev. Lett.* **99** (2007) 192301 [[hep-ph/0703082](#)].
- [38] J.-P. Blaizot, E. Iancu and Y. Mehtar-Tani, *Medium-induced QCD cascade: democratic branching and wave turbulence*, *Phys. Rev. Lett.* **111** (2013) 052001 [[1301.6102](#)].
- [39] J.-P. Blaizot, F. Dominguez, E. Iancu and Y. Mehtar-Tani, *Probabilistic picture for medium-induced jet evolution*, *JHEP* **06** (2014) 075 [[1311.5823](#)].
- [40] P. B. Arnold, *Simple Formula for High-Energy Gluon Bremsstrahlung in a Finite, Expanding Medium*, *Phys.Rev.* **D79** (2009) 065025 [[0808.2767](#)].
- [41] Y. Mehtar-Tani and S. Schlichting, *Universal quark to gluon ratio in medium-induced parton cascade*, *JHEP* **09** (2018) 144 [[1807.06181](#)].
- [42] R. Baier, A. H. Mueller, D. Schiff and D. T. Son, *'Bottom up' thermalization in heavy ion collisions*, *Phys. Lett.* **B502** (2001) 51 [[hep-ph/0009237](#)].
- [43] A. Kurkela, A. Mazeliauskas, J.-F. Paquet, S. Schlichting and D. Teaney, *Effective kinetic description of event-by-event pre-equilibrium dynamics in high-energy heavy-ion collisions*, *Phys. Rev.* **C99** (2019) 034910 [[1805.00961](#)].
- [44] J.-P. Blaizot, F. Dominguez, E. Iancu and Y. Mehtar-Tani, *Medium-induced gluon branching*, *JHEP* **01** (2013) 143 [[1209.4585](#)].
- [45] L. Apolinário, N. Armesto, J. G. Milhano and C. A. Salgado, *Medium-induced gluon*

radiation and colour decoherence beyond the soft approximation, *JHEP* **02** (2015) 119 [[1407.0599](#)].

- [46] J.-P. Blaizot and Y. Mehtar-Tani, *Energy flow along the medium-induced parton cascade*, *Annals Phys.* **368** (2016) 148 [[1501.03443](#)].
- [47] R. Baier, Y. L. Dokshitzer, A. H. Mueller and D. Schiff, *Quenching of hadron spectra in media*, *JHEP* **0109** (2001) 033 [[hep-ph/0106347](#)].
- [48] M. Spousta and B. Cole, *Interpreting single jet measurements in Pb + Pb collisions at the LHC*, *Eur. Phys. J.* **C76** (2016) 50 [[1504.05169](#)].
- [49] Y. Mehtar-Tani and K. Tywoniuk, *Sudakov suppression of jets in QCD media*, *Phys. Rev.* **D98** (2018) 051501 [[1707.07361](#)].